Electrochimica Acta 209 (2016) 661–670

Contents lists available at ScienceDirect

Electrochimica Acta

journal homepage: www.elsevier.com/locate/electacta

Platinum-based nitrogen-doped porous C_xN_{1-x} compounds used as a transducer for sensitive detection of hydrogen peroxide

Xiaomin Lei[1], Tingting Li[1], Yunpeng Zuo, Wenmin Yin, Long Wu, Kang Shao, Xiaoyan Xiao, Zhicheng Lu, Heyou Han*

State Key Laboratory of Agricultural Microbiology, College of Science, Huazhong Agricultural University, Wuhan 430070, China

ARTICLE INFO

Article history:
Received 25 January 2016
Received in revised form 3 April 2016
Accepted 18 May 2016
Available online 19 May 2016

Keywords:
Platinum-based nanoparticles
porous carbon
nitrogen-doped
peroxidase-like activity
electrocatalysis

ABSTRACT

Functional platinum-based carbonous nanostructures play important roles in exploring new electrode materials by constructing sensitive and selective platform in the electrochemical detection. In recent years, intense research efforts have focused on boosting the performance of platinum with desirable activity and stability. This work reports a facile strategy for the synthesis of platinum-based nitrogen-doped porous C_xN_{1-x} compounds (Pt-pC_xN_{1-x}) with excellent enzyme-like activity. In the strategy, Pt-pC_xN_{1-x} was simply prepared by in situ synthesis through a one-step microwave-assisted heating procedure, resulting with subnanometer-size (~2.5 nm) platinum-based nanoparticles (Pt-BNPs) loaded on the multi-dimensional C_xN_{1-x} structure. Due to the enriched edge and corner atoms, Pt-pC_xN_{1-x} showed excellent intrinsic peroxidase-like activity. Meanwhile, it was demonstrated that Pt-pC_xN_{1-x} possessed a lower Michaelis Constant (K_m = 0.104) compared with horseradish peroxidase (HRP) (K_m = 0.416) in the presence of 3,3,5,5-tetramethylbenzidine (TMB) and hydrogen peroxide (H_2O_2). Moreover, the Pt-pC_xN_{1-x} behaved better property and lower cost in H_2O_2 electrochemical detection compared with the pC_xN_{1-x} and Pt-BNPs. The detection results exhibited a low detection limit (2.29 μM) and a wide linear range (0.025 to 5.725 mM), which revealed its superior potential in H_2O_2 electrochemical detection. Therefore, the Pt-pC_xN_{1-x} may find a potential application in constructing electrochemical biosensors.

1. Introduction

Currently, intense interest has been paid to loading various nanoparticles or alloys on graphite-like carbon compounds as enzyme mimetics for a wide range of biomedical, sensor and technological applications [1–8]. Among known nanomaterials, platinum-based nanoparticles (Pt-BNPs) have attracted particular attention due to their various advantages over natural enzymes against denaturation or protease digestion [9–12]. However, the activity of Pt-BNPs catalysts has been influenced by many factors, for example, the size, distribution and stability of Pt-BNPs and the support materials [13–15]. According to prior research, the most favorable size for Pt-BNPs catalysts is within the range of 10 nm [16]. Unfortunately, the catalysts could easily aggregate in this size range due to the large surface energy, which lead to the decrease of the catalytic activity. Hence, it is essential to screen ideal materials to stabilize the nanoscale Pt-BNPs to enhance their utilization.

As the candidate materials to support Pt-BNPs, some kinds of graphitic carbon materials such as graphene, carbon nanofibers, ordered mesoporous carbon, carbon nanotubes have been studied [1,17,18]. Yan et al. prepared polydopamine-coated ordered mesoporous carbons to load well-dispersed Pt nanoparticles for H_2O_2 electrochemical reduction and exhibited improved electrocatalytic activity, and that polydopamine on the ordered mesoporous carbons facilitated the obtainment of ultra-fine Pt nanoparticles with good dispersion and small particle size [19]. Liu et al. developed a novel biosensor based on highly exposed Pt nanoparticles decorated porous graphene for the reliable detection of extracellular H_2O_2, which showed good performance toward the electrocatalytic reduction of H_2O_2 [20]. Among numerous support materials, porous carbons have been attracting more and more attention because of their outstanding characteristics such as high surface area, good electrical conductivity, multi-channel for ion transport/diffusion and electronic transmission path, and intensified electrolyte permeability [21–24]. However, the excellent performance of porous carbons not only depends on the surface structure and porosity derived from raw materials, but also depends on the heteroatoms doped in their structures [25,26]. The

* Corresponding author: Tel.: +86 27 87282043; fax: +86 27 87282043.
E-mail address: hyhan@mail.hzau.edu.cn (H. Han).
[1] These authors contributed equally to this work.

http://dx.doi.org/10.1016/j.electacta.2016.05.131
0013-4686/

introduced heteroatoms, especially the nitrogen with five valence electrons, can effectively tune the electronic characteristics and enhance the electronic conductivity, providing hydrophilic ability and basic properties to increase the functionality of carbon [25,27–29]. And the doping of nitrogen could also facilitate the well dispersion and immobilization of ultrafine Pt-BNPs by increasing surface defects to serve as Pt-BNPs nucleation sites [30,31]. In addition, the nitrogen has influence on the binding of the Pt-BNPs to the carbon support by altering the electron donating feature of carbon support, which could prevent Pt-BNPs from agglomerating and coarsening [30]. Thus, the nitrogen-doped porous C_xN_{1-x} compounds (pC_xN_{1-x}) were perceived as a promising candidate for a variety of applications in the fields of physical chemistry [32,33]. Compared to graphene-like carbon compounds [25,34], pC_xN_{1-x} is lower in cost and easier in preparation. It is also have been studied that nitrogen doped carbon materials itself display attractive electrocatalytic activity for reduction of H_2O_2 [28,35]. The aforementioned advantages of pC_xN_{1-x} suggest its great potential as a prominent support material.

As the reactive oxygen species and by-products of many reactions contain oxidase enzymes, H_2O_2 as a signal molecule plays an indispensable role in adjusting different biological processes. With the development of nanotechnology in recent years, it is essential to establish some simple and rapid methods for the detection of H_2O_2. The colorimetric detection was firstly performed to test the peroxidase-like catalytic activity of Pt-pC_xN_{1-x} in catalyzing the oxidation of 3,3′,5,5′-tetramethylbenzidine (TMB) by H_2O_2,revealing that Pt-pC_xN_{1-x} has excellent peroxidase-like activity. Furthermore, on the basis of the fast response and high sensitivity as well as low-cost and convenient operation for actual applications [1,36], the electrochemical method was also adopted to investigate the analysis of H_2O_2. The results revealed that Pt-pC_xN_{1-x} displayed remarkable electrocatalytic activity and stability. So in our work, a novel nonenzymatic sensor based on Pt-pC_xN_{1-x} was the first time to be fabricated for sensitive detection of H_2O_2, and the support pC_xN_{1-x} was easily prepared through one-step cross-linking reaction of melamine and formaldehyde without any extrinsic nitrogen source. The good catalytic activity of this nanocomposite is depend on its special composition and structure. Firstly, the porous structure and large surface area are beneficial to the loading of plentiful Pt-BNPs. Then the doping of nitrogen atoms can alter electron character of carbon support and facilitate the anchoring and dispersion of Pt-BNPs. The last but not the least, pC_xN_{1-x} and subnanometer-size Pt-BNPs provide synergistic effects on the catalytic performance of H_2O_2 electrochemical reduction.

2. Experimental Section

2.1. Reagents and Apparatus

Melamine (99.5%) was purchased from Tianjin Guangfu Fine Chemical Research Institute. Formaldehyde, sodium hydrate (NaOH, AR), hydrochloric acid (HCl, AR), ethylene glycol (AR), hydrogen peroxide (H_2O_2, 30%, AR), chloroplatinic acid hexahydrate ($H_2PtCl_6{\cdot}6H_2O$, AR), sodium acetate (NaAc, AR), acetic acid (HAc, AR), chitosan (AR) was obtained from Sinopharm Chemical Reagent Co., Ltd. Hydrophilic nano-$CaCO_3$ was purchased from Shanxi Xintai NanoMater. 3,3',5,5'-tetramethylbenzidine (TMB, 99%) was acquired from Sigma-Aldrich. Ultrapure water with a conductivity of 18.25 MΩ-cm was used in the whole experiment process. Unless special instructions, other chemicals were of analytical reagent and used without further purification.

Scanning electron microscopy (SEM) images and SEM-EDS mapping were carried out on a JEOL JSM–6700F field emission scanning electron microscope. Transmission electron microscopy (TEM) and high-resolution transmission electron microscopy (HRTEM) measurements were performed on a JEM-2010FEF high-resolution transmission electron microscope at an accelerating voltage of 200 kV. The X-ray diffraction (XRD) measurement was made on a Bruker D8 Advance X-ray diffractometer with Cu Kα radiation. The X-ray photoelectron spectra (XPS) were measured using a Thermo VG Multilab 2000 spectrometer equipped with a monochromatic Al Kα radiation source at room temperature. The Raman spectras were recorded by a Renishaw inVia Raman spectrometer equipped with a He-Ne laser excitation source operating at 632.8 nm. Nitrogen adsorption/desorption measurements were carried out by Brunauer–Emmett–Teller (BET) technique using a Micromeritics ASAP 2460 M automated sorption analyzer. The pore size distribution was determined by desorption date using Barrett–Joyner–Halenda (BJH) method. Thermal gravimetric analysis (TGA) measurements were performed on a NETZSCH TG 209C thermobalance with a heating rate of 10 °C min^{-1} under air and a flow rate of 20 cm^3 min^{-1}. Ultraviolet-Visible (UV-Vis) absorption spectra were recorded on PerkinElmer Lambda 25 Ultraviolet-Visible spectrometer. Electrochemical measurements were performed by a CHI 660D electrochemical workstation.

2.2. Preparation of nitrogen-doped porous C_xN_{1-x} (pC_xN_{1-x})

The pC_xN_{1-x} was prepared as reported in our previous work [33] with some modifications. In a typical experiment, melamine (31.5 g) was added to the stirring solution of formaldehyde (50 mL) at room temperature, and the pH value of the mixure was adjusted to 8-9 by adding diluted NaOH, followed by stirring at 80 °C for 20 min to obtain a clear solution. Then, the pH value of the mixture was adjusted to 5-6 by adding diluted HCl, followed by the addition of hydrophilic nano-$CaCO_3$ (40 g) under vigorous stirring. Meanwhile, a small amount of water was added to prepare a homogenous solution under constant stirring until the solution was solidified. Subsequently, the solid product was dried at 60 °C in the air and heated slowly to 180 °C overnight. The resultant composite was carbonized at 900 °C for 2 h at the heating rate of 5 °C min^{-1} under the protection of nitrogen flow. After cooling to room temperature, the obtained CaO/nitrogen-doped carbon composites were ground to fine powders and stirred in diluted HCl solution for 24 h. Finally, the product was separated through suction filtration, washed several times with deionized water, and dried in a vacuum oven at 150 °C for 10 h. The as-prepared product was named as pC_xN_{1-x}.

2.3. Synthesis of Pt-based porous C_xN_{1-x} compound (Pt-pC_xN_{1-x})

In a typical synthesis, 20 mg of pC_xN_{1-x} was dispersed in 10 mL of ethylene glycol with ultrasonication, followed by the addition of an aqueous solution of 1 mL of H_2PtCl_6 (0.02 M), then the pH of mixure was adjusted to 8-9 by adding diluted KOH and stirring to obtain well-mixed solution. After ultrasonic treatment for approximately 30 min, the mixture was placed in a microwave oven with programmed heating-up to 120 °C for 20 min (power: 400 W). Then the resultant solution was cooled naturally to the room temperature, isolated by centrifugal separation, washed several times with deionized water until the upper liquid was clear, and then freeze-dried overnight. The final resultant nanocomposite was labeled as Pt-pC_xN_{1-x}.

2.4. Assay of peroxidase-like activity

The assays of peroxidase-like activity were carried out in time-drive mode by monitoring the absorbance change at 652 nm for 5 min on a UV-visible spectrophotometer at room temperature.

Experiments were carried out using 3.0 μg mL^{-1} nanomaterial in a reaction volume of 1 mL NaAc buffer solution (0.2 M, pH = 3.5) containing 0.8 mM TMB as substrate, at the H_2O_2 concentration of 50 mM, unless otherwise stated. The Michaelis-Menten constant was calculated using Lineweaver-Burk plots to obtain the double reciprocal of the Michaelis-Menten equation, $1/\nu = (K_m/V_{max})\cdot(1/[S] + 1/K_m)$, where ν is the initial velocity, V_{max} represents the maximum initial velocity, [S] corresponds to the concentration of the substrate, and K_m is known as the Michaelis–Menten constant [11,37].

2.5. Electrochemical measurements

The electrochemical measurements were performed on a CHI 660D electrochemical workstation (Chen Hua Co., China) using a three electrode system, with a modified glassy carbon electrode (GCE) (3 mm diameter) as a working electrode, a platinum wire as a counter electrode, and an Ag/AgCl (in saturated KCl solution) electrode as a reference electrode. Before modification, GCE was polished separately with 1.0, 0.3 and 0.05 μm alumina slurry and washed ultrasonically in ultrapure water and ethanol for a few minutes, then dried with high-purity nitrogen flow. Pt-pC_xN_{1-x}-modified GCE was prepared by casting 5.0 μL of the Pt-pC_xN_{1-x} suspension (1 mg mL^{-1}) onto the GCE surface, followed by sealing with 5.0 μL 0.05 wt% chitosan solution and drying in air at room temperature. For comparison, bare GCE, pC_xN_{1-x}-modified GCE and Pt-BNPs-modified GCE were prepared using the same method. The electrolyte solution was purged with pure N_2 for 15 min to remove oxygen before the electrochemical measurement.

3. Results and Discussion

3.1. Material Synthesis and Characterization

Pt-pC_xN_{1-x} was synthesized by decorating subnanometer-size Pt-BNPs on the surface of pC_xN_{1-x} (Scheme 1). As illustrated in Scheme 1, the pC_xN_{1-x} was obtained as previously reported[33]. The nitrogen-doping porous structure can provide a powerful support for immobilizing platinum nanoparticles[38,39]. Finally, the combination of ultrafine and homodispersed Pt-BNPs on the surface of pC_xN_{1-x} was carried out through an in situ reduction of H_2PtCl_6 to acquire the Pt-pC_xN_{1-x} nanocomposites.

Fig. 1a and 1b show the SEM images of pC_xN_{1-x} and Pt-pC_xN_{1-x}, the porous and stratiform structure can be seen clearly from images. The pure structure of pC_xN_{1-x} could be clearly distinguished from Fig. 1a_1. The enlarged HRTEM images of Pt-pC_xN_{1-x} as shown in Fig. 1b_1 and 1c reveal that subnanometer-size Pt-BNPs are evenly distributed on the surface of pC_xN_{1-x}. And the nitrogen atoms doped in the pC_xN_{1-x} are able to prevent Pt-BNPs from aggregation due to the interaction between the electrons of Pt-BNPs and nitrogen atoms [38–40]. The obtained Pt-BNPs are close to 2.5 nm in size as shown in the upper right corner of Fig. 1c. From the HRTEM and filtered images shown in Fig. 1d, it is clear that the d-spacing of adjacent fringes for the subnanometer-size Pt-BNPs is 0.23 nm, which corresponds to the (111) planes of a face-centered cubic (*fcc*) Pt [1].

As depicted in SEM images (Fig. 2a and 2b), the elemental mapping selected area could reflect the distribution of elements in the material. The SEM-EDS mapping images (Fig. 2c-2f) exhibit the chemical composition, highlighting the distribution of elements (C, N, O, Pt-BNPs marked with different colors) within the Pt-pC_xN_{1-x}. The elemental mapping results reveal that the C, N, O are effectively and uniformly incorporated into the Pt-pC_xN_{1-x}, and Pt-BNPs are also uniformly distributed onto the materials.

The XRD patterns of pC_xN_{1-x} in Fig. 3a show two diffraction peaks at around 43.0° and 25.9°, which can be indexed to the (101) and (002) planes of pC_xN_{1-x} [20], respectively. All the peaks related to Pt shown in the XRD patterns of Pt-C_xN_{1-x} can be assigned to *fcc* Pt, which is consistent with the standard literature values (JCPDS no.04-0802). Meanwhile, with the loading of Pt-BNPs, the diffraction peak (101) of pC_xN_{1-x} gradually decreases, revealing that the distribution of Pt-BNPs is probably related to nitrogen, which could also be verified by XPS (Fig. 3b). When the carbon material is loaded with Pt-BNPs, the bulk material exhibits the XPS peak of Pt_{4f} [8] instead of pC_xN_{1-x}. Additionally, the binding energy of N 1s in Pt-pC_xN_{1-x} is larger than that in pC_xN_{1-x}, further confirms that the loading of Pt-BNPs on pC_xN_{1-x} is related to N. The shift of the binding energy of N 1s indicates that partial nitrogen atoms are changed to oxidation state, which might facilitate the synthesis of Pt-BNPs in situ. The ratios of the integrated D-band (~1,330 cm^{-1}) and G-band (~1,580 cm^{-1}) intensities in Raman spectra (Fig. 3c) are 1.104 and 1.016, which could be ascribed to pC_xN_{1-x} and Pt-pC_xN_{1-x}, respectively. The intensity ratio can reflect the degree of graphitization of materials, the smaller the ratio then the higher the degree of graphitization.The Raman results reflect that the graphitization degree of Pt-pC_xN_{1-x} is higher than pC_xN_{1-x}, which indicates the superior electric conductivity of Pt-pC_xN_{1-x} [41]. On the other side, it is also explained the number of defective sites decreased [42], resulting from the loading of Pt-BNPs. All the above analysis results confirmed that the Pt-BNPs were loaded on the pC_xN_{1-x} with a stable structure.

The TGA as a kind of analysis method can also verify the attachment Pt-BNPs to pC_xN_{1-x} and obtain the estimated amount of Pt-BNPs (Fig. S1). As shown in Fig. S1, the temperature range of main weight loss for pC_xN_{1-x} is between 500 °C and 670 °C, which comes from the thermal decomposition of pC_xN_{1-x} in air atmosphere and residue mass close to zero. The temperature range of main weight loss for Pt-pC_xN_{1-x} is between 350 °C and 620 °C, and its residue mass remain about 20%. The difference between pC_xN_{1-x} and Pt-pC_xN_{1-x} further verified that Pt-BNPs are successfully attached to pC_xN_{1-x}, which is consistent with the above results. The weight ratio of the Pt-BNPs to pC_xN_{1-x} is

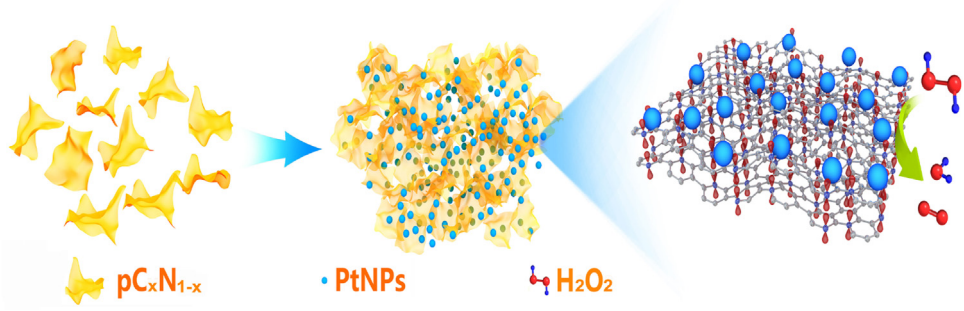

Scheme 1. Schematic illustration of the synthesis of Pt-pC_xN_{1-x}.

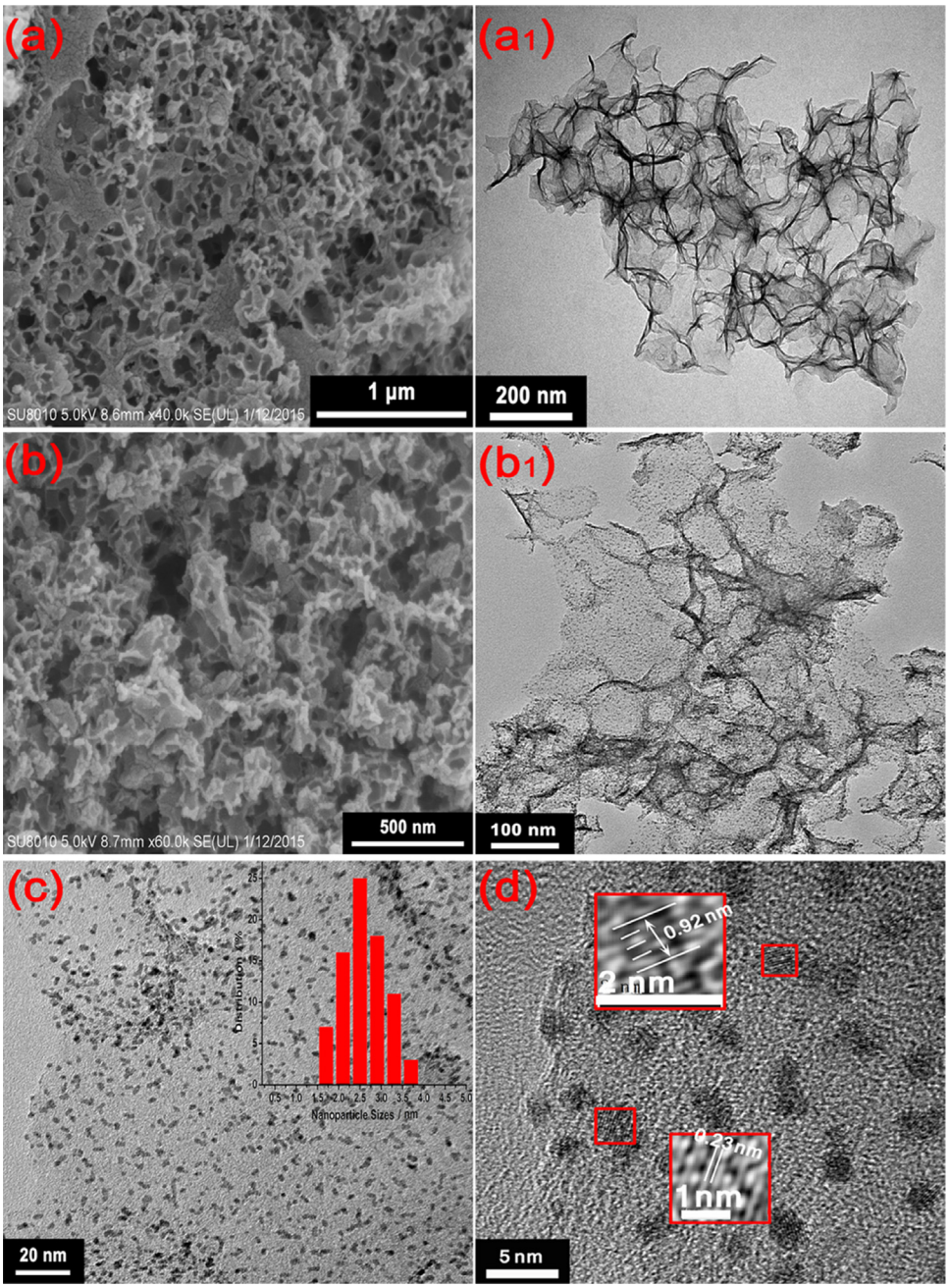

Fig. 1. (a, b) SEM images of pC_xN_{1-x} (a)and Pt-pC_xN_{1-x} (b);(a_1, b_1) TEM images in accordance with (a, b). (c) The enlarged HRTEM images of Pt-pC_xN_{1-x} and the size distribution of Pt-BNPs (inset in the upper right corner of (c)). (d) HRTEM and filtered images of the square area.

estimated to be 0.23: 0.77. Fig. S2 presents the nitrogen adsorption–desorption isotherms of pC_xN_{1-x} and Pt-pC_xN_{1-x}. The obtained isotherm exhibited type II with H3 type hysteresis loop and a pronounced capillary condensation step at high relative pressure range, indicating the existence of plentiful mesopores and macropores. The specific surface area and pore volume of pC_xN_{1-x} are 370.90 m^2g^{-1} and 2.65 cm^3g^{-1}, which facilitate the attachment of Pt-BNPs and offer a large reaction interface. Also, pore size distributions of pC_xN_{1-x} are exhibited in inset of Fig. S2a, which elucidate that pC_xN_{1-x} own varying sizes of nanopores. The specific surface area and pore volume of Pt-pC_xN_{1-x} are 199.80 m^2g^{-1} and 1.90 cm^3g^{-1}, which reflect the specific surface area of Pt-pC_xN_{1-x} is less than that of pC_xN_{1-x}. The reasons for this difference were the collapse of some holes caused by the ultrasonic process and the coverage of some micropores or small mesopores caused by the loading of platinum nanoparticles, which greatly reduced micropores and then leading to the decrease of specific surface area. The result of pore size distribution of Pt-pC_xN_{1-x} is in conformity with it (Fig. S2b). However, most of the holes are still exist, and three-dimensional structure composed of interconnected holes could still be observed from SEM images of Pt-pC_xN_{1-x}.

3.2. Kinetics analysis of peroxidase-like catalytic activities of Pt-pC_xN_{1-x} nanocomposites

The catalytic oxidation of TMB by Pt-pC_xN_{1-x} was investigated in the presence or absence of H_2O_2 using pC_xN_{1-x} and Pt-BNPs as a comparison. As shown in Fig. 4a, TMB could be easily oxidized in the presence of Pt-pC_xN_{1-x} and H_2O_2 with a rapid color change from nearly colourless to blue (a7). However, no significant color

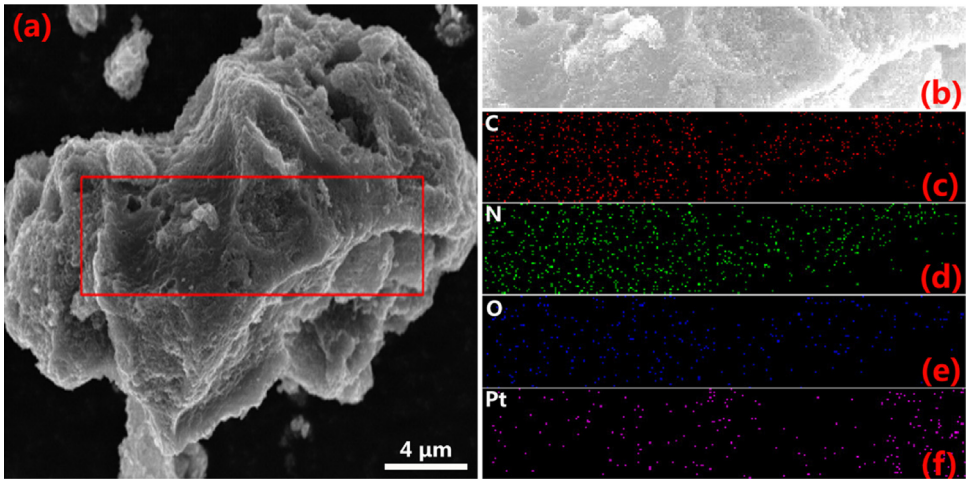

Fig. 2. (a) The field-emission scanning electron microscopy (FESEM) of Pt-pC_xN_{1-x}; (b) FESEM of the analyzed area labeled with red rectangle in (a); (c,d,e,f) SEM-EDS mapping from the same area for C, N, O, Pt-BNPs marked with different colors from top to bottom.

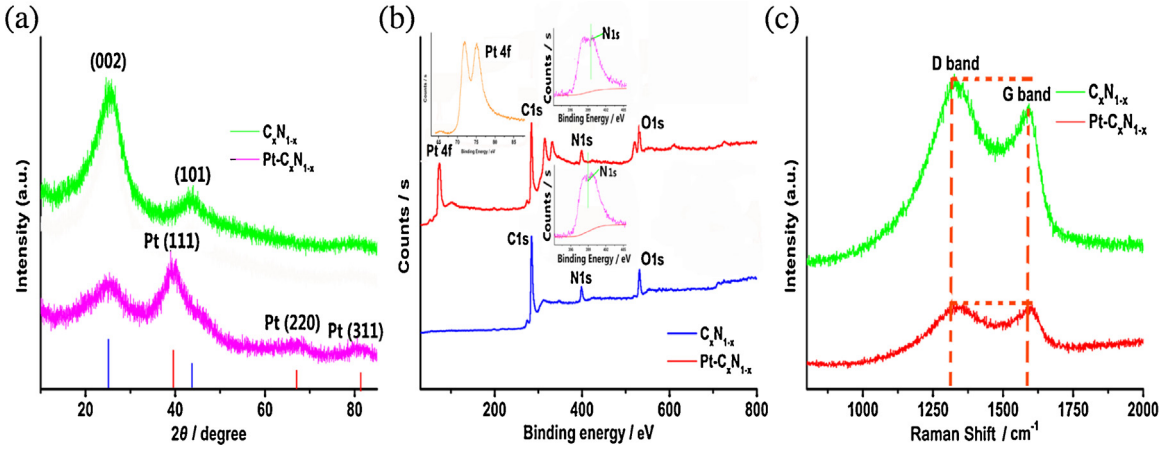

Fig. 3. (a) The X-ray diffraction (XRD) pattern; (b) X-ray photoelectron spectroscopy (XPS) of pC_xN_{1-x} and Pt-pC_xN_{1-x}; (c) Raman spectra of pC_xN_{1-x} and Pt-pC_xN_{1-x} with D and G bands.

change was observed by the naked eye in the TMB + H_2O_2 (a1) or TMB + Pt-pC_xN_{1-x} (a4) solution. The pC_xN_{1-x} also presented the similar result to that of Pt-pC_xN_{1-x}, which is also consistent with other reported carbon materials [34,37,43]. It is known to all that Pt-BNPs has high catalytic activity in catalyzing oxidation of TMB in the presence of H_2O_2 [9,11]. It is worth noting that the blue color density produced by Pt-pC_xN_{1-x} was higher than that obtained from pC_xN_{1-x} and Pt-BNPs, and the UV absorption values at 652 nm and 370 nm were the highest. These results confirmed that all the three nanomaterials possessed the intrinsic peroxidase-like catalytic activity, and Pt-pC_xN_{1-x} nanocomposites could exhibit greatly enhanced peroxidase-like catalytic activity in contrast to the component materials.

To further discuss the differences between the three nanomaterials (pC_xN_{1-x}, Pt-BNPs, Pt-pC_xN_{1-x}), the time-dependent absorbance changes at 652 nm within 5 min were recorded by UV–vis spectra. Fig. 4b-4d show the time-dependent absorbance changes at 652 nm in different reaction systems with different catalyst concentrations ranging from 0.0 to 3.0 μg mL^{-1}. As shown in Fig. 4b and 4c, the absorbance of the oxidation product of TMB (800 μM) based on pC_xN_{1-x} and Pt-BNPs increased with the increasing concentration of the catalyst, but still maintained an upward tendency when the concentration reached 3.0 μg mL^{-1}. In the catalyst-TMB-H_2O_2 system (800 μM TMB, 50 mM H_2O_2), the absorbance intensities of Pt-pC_xN_{1-x} increased much more rapidly than those of pC_xN_{1-x} and Pt-BNPs and reached equilibrium at the concentration of 3.0 μg mL^{-1}. These results demonstrated that Pt-pC_xN_{1-x} possessed higher catalytic activity after compounding in composites. As a result, 3.0 μg mL^{-1} was chosen as the optimal catalyst concentration for reaction in the following experiments.

Moreover, the peroxidase-like activities of pC_xN_{1-x}, Pt-BNPs and Pt-pC_xN_{1-x} nanocomposites were also explored by analyzing the steadystate kinetics of TMB oxidation reaction. Typical Michaelis–Menten curves were achieved in a certain range of H_2O_2 or TMB concentrations (Fig. S3). With the Lineweaver–Burk equation [44], the K_m and the V_{max} were obtained and shown in Table S1. The apparent K_m value of Pt-pC_xN_{1-x} (0.108 mM) with the TMB substrate was lower than that of pC_xN_{1-x} (0.577 mM), or Pt-BNPs (0.713 mM) and about one quarter that of HRP (0.434 mM), which suggested that the Pt-pC_xN_{1-x} could perform a higher affinity with TMB. Additionally, the V_{max} of the Pt-pC_xN_{1-x} (52.712×10^{-8} M s^{-1}) with TMB as the substrate was five-fold that of HRP (10.00×10^{-8} M s^{-1}) [44], which favoring a higher reaction rate than HRP. The apparent K_m of the Pt-pC_xN_{1-x} with the H_2O_2 substrate was also lower than that of pC_xN_{1-x} or Pt-BNPs, indicating that Pt-pC_xN_{1-x} had a higher affinity for H_2O_2. These results showed that Pt-pC_xN_{1-x} had superior peroxidase-like activity to the pure Pt-BNPs and pC_xN_{1-x} and behave comparable catalytic performance to natural

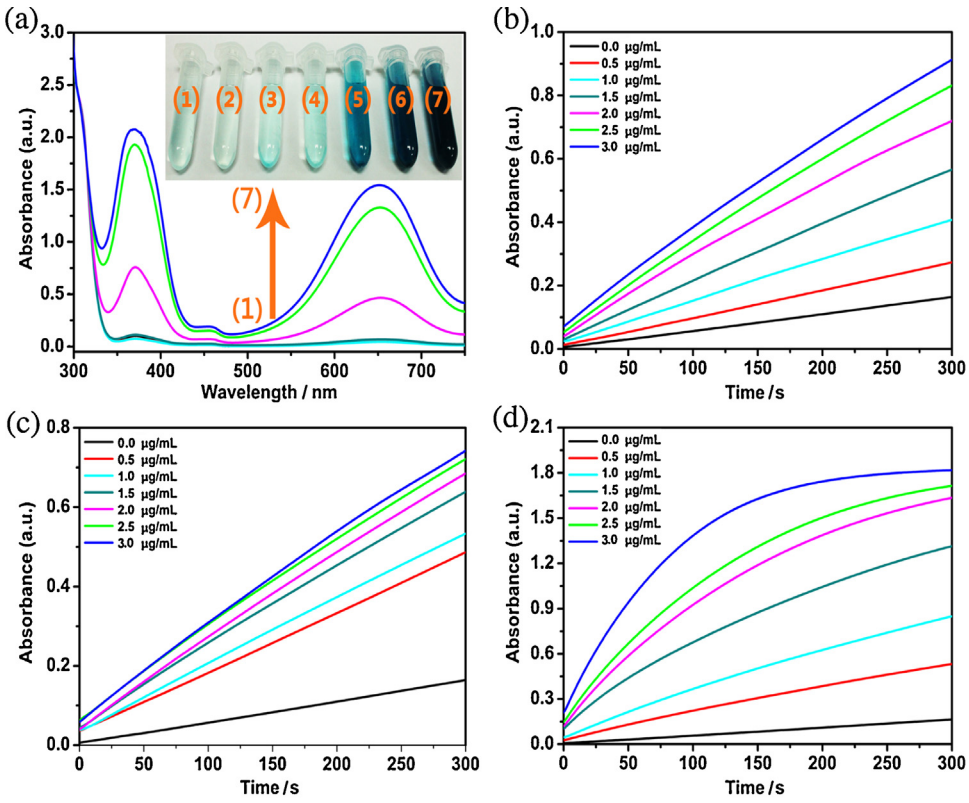

Fig. 4. (a) UV–vis spectra of TMB (800 μM) mixed with H_2O_2 (50 mM) (a1), pC_xN_{1-x} (a2), Pt-BNPs(a3), Pt-pC_xN_{1-x} (a4), pC_xN_{1-x} and H_2O_2 (50 mM) (a5), Pt-BNPs and H_2O_2 (50 mM) (a6), Pt-pC_xN_{1-x} and H_2O_2 (50 mM) (a7). Inset: Typical photographs of different solutions corresponding to (a1)-(a7) in 0.2 M, pH = 3.5 NaAc buffer. The time-dependent absorbance (A652) of different concentrations (0.0 to 3.0 μg/mL) of (b) pC_xN_{1-x}, (c) Pt-BNPs, (d) Pt-pC_xN_{1-x} in presence of TMB (800 μM) and H_2O_2(50 mM).

enzymes. Moreover, Pt-pC_xN_{1-x} may overcome the intrinsic problems of natural enzymes such as poor stability and harsh experimental conditions [10], thus it could also be utilized to take place of enzymes and play a role in biological sensing/detection.

The excellent peroxidase-like activity of Pt-pC_xN_{1-x} can be mainly ascribed to its unique structure. Meanwhile, the TMB molecules absorbed on the surface of the Pt-pC_xN_{1-x} could donate lone pair electrons in the amino groups to further increase the electron density and mobility [37], and thus accelerates the electron transfer from Pt-pC_xN_{1-x} to H_2O_2. What is more, the ultrafine Pt-BNPs were uniformly distributed on the surface of pC_xN_{1-x} which could offer more surface active sites to catalyze H_2O_2.

3.3. Electrocatalytic behaviors of Pt-pC_xN_{1-x} towards H_2O_2

Cyclic voltammetry, a convenient, simple and sensitive method is often used to characterize the catalytic activities of the as-synthesized electrodes. Fig. S4 shows the Cyclic Voltammograms (CVs) of bare GCE, pC_xN_{1-x}-modified GCE, Pt-BNPs-modified GCE and Pt-pC_xN_{1-x}-modified GCE in potassium ferricyanide solution containing 0.5 M KCl and 5 mM $K_3[Fe(CN)_6]$. As shown in Fig. S4, all of these electrodes presented a pair of well-defined oxidation and reduction peaks owing to the $[Fe(CN)_6]^{3-/4-}$ redox couple. Expectly, pC_xN_{1-x}-modified GCE and Pt-BNPs-modified GCE show an increase in the peak current as compared with the bare GCE, indicating that pC_xN_{1-x} and Pt-BNPs have a certain conductive ability. Moreover, Pt-pC_xN_{1-x}-modified GCE shows a higher increase in peak current, but its peak potentials remain very narrow on the basis of pC_xN_{1-x} and Pt-BNPs, which indicating that the conductive ability of Pt-pC_xN_{1-x} increases greatly after the compounding of materials. The average electroactive surface areas could also be calculated from CVs according to the Randles–Sevcik equation [45], $I_p = 2.69 \times 10^5 \times A \times D^{1/2} \times n^{3/2} \times V^{1/2} \times C$, where I_p is the redox peak current, A is the area of the electroactive surface area (cm^2), D is related to the diffusion coefficient of the molecule in solution and is about $(6.70 \pm 0.02) \times 10^{-6}\,cm^2\ s^{-1}$, n is the number of electrons participating in the redox reaction (for $[Fe(CN)_6]^{3-/4-}$, n = 1), C presents the bulk concentration of the redox probe (mol cm^{-3}) and V corresponds to the scan rate (Vs^{-1}) of the potential perturbation. According to the above equation, the surface areas of electrodes were calculated and the results follow the trend of bare GCE ($0.0619\,cm^2$) < pC_xN_{1-x} ($0.0732\,cm^2$) < Pt-BNPs($0.0740\,cm^2$) < Pt-pC_xN_{1-x} ($0.0800\,cm^2$), revealing that Pt-pC_xN_{1-x} had higher electroactive surface areas than pC_xN_{1-x} or Pt-BNPs. The above results may be attributed to the stable porous structure of pC_xN_{1-x} and the numerous well-distributed ultrafine Pt-BNPs on the surface of pC_xN_{1-x}. In addition, the electrochemical impedance spectroscopy (EIS) is also an effective electrochemical measurement method to acquire more information about the structure of the electrode interface and other dynamic information [46,47]. Fig. 5 shows the Nyquist plots obtained for bare GCE (the dark), pC_xN_{1-x}-modified GCE (the red), Pt-BNPs-modified GCE (the blue) and Pt-pC_xN_{1-x}-modified GCE (the dark cyan) in 0.5 M KCl solution containing 5 mM $[Fe(CN)_6]^{3-/4-}$. The resistances of charge transfer (R_{ct}) for the bare GCE, pC_xN_{1-x}-modified GCE, Pt-BNPs-modified GCE and Pt-pC_xN_{1-x}-modified GCE were estimated to be 175 Ω, 97 Ω, 126 Ω and 48 Ω, respectively. The results indicated that pC_xN_{1-x}-, Pt-BNPs- and Pt-pC_xN_{1-x}-modified electrodes possessed higher conductivity and facilitated the charge transfer, which was consistent with the result of cyclic voltammetry. However, Pt-pC_xN_{1-x}-modified electrode possessed the lowest R_{ct}

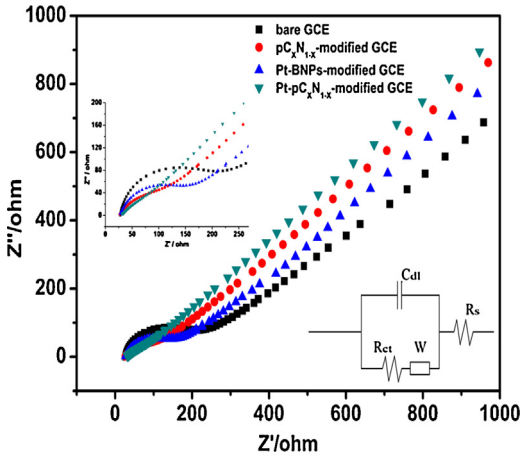

Fig. 5. Nyquist plots for bare GCE, pC_xN_{1-x}-modified GCE, Pt-BNPs-modified GCE and Pt-pC_xN_{1-x}-modified GCE measured in 0.5 M KCl solution containing 5 mM $[Fe(CN)_6]^{3-/4-}$ (frequency range 100 kHz-0.1 Hz, perturbation signal 5 mV, OCP). The inset is the fits of equivalent circuit.

among all the electrodes because Pt-BNPs and pC_xN_{1-x} played a synergistic role in improving electrocatalytic conductivity of nanocomposites.

The CVs of the electrochemical response to H_2O_2 at different electrodes were presented in Fig. 6. Nearly no redox peaks can be observed at bare GCE after the addition of 2 mM H_2O_2 (Fig. 6a), suggesting that the electrocatalytic activity of bare GCE to H_2O_2 reduction was restrained because of its slow electrode kinetics and high overpotential [46]. Compared with bare GCE, an increase of the reduction peak current can be observed obviously for pC_xN_{1-x}-modified GCE upon addition of 2 mM H_2O_2 (Fig. 6b), indicating a certain catalytic ability of pC_xN_{1-x} to H_2O_2 with a slightly wide peak. In contrast, Pt-BNPs-modified GCE (Fig. 6c) exhibited a significant increase on the reduction peak current with a very narrow peak compared with bare GCE. At the same time, a cathodic current at about 0.02 V was obtained separately on the Pt-BNPs-modified GCE (Fig. 6c) and Pt-pC_xN_{1-x}-modified GCE (Fig. 6d), due to the reduction of platinum oxide, demonstrating that Pt-BNPs were successfully attached to the modified electrode [46]. Additionally, the maximum reduction peak current of Pt-pC_xN_{1-x}-modified GCE was much higher than that of bare GCE, pC_xN_{1-x}-modified GCE, or Pt-BNPs-modified GCE, indicating its higher electrocatalytic activity toward the reduction of H_2O_2. The results further demonstrated that Pt-pC_xN_{1-x} can be used as an excellent material for H_2O_2 detection. In addition, there is a relationship between the loading level of Pt-BNPs and electrocatalytic activity of Pt-pC_xN_{1-x}. Fig. S5 shows the TEM images and electrochemical testing results of various levels of Pt-BNPs on pC_xN_{1-x}, and the mass ratios are based on addition amounts of pC_xN_{1-x} and Pt-BNPs. As shown from Fig. S5a to Fig. S5c, high levels of Pt-BNPs would obtain the large size of Pt-BNPs or the aggregation of Pt-BNPs, and their catalytic currents increased slowly compared with 1: 0.195 (Fig. 2d) which used in this work. But low levels of Pt-BNPs can't obtain high catalytic activity due to less of active sites, as reflected in Fig. S5e to Fig. S5h. Taken the cost and electrochemical properties in consideration, the level of Pt-BNPs which we prepared in this work was optimal to construct the non-enzyme electrochemical sensor for the following electrochemical detection.

Fig. 7a shows the typical CVs of Pt-pC_xN_{1-x}-modified GCE in N_2-saturated 0.1 M PBS solution (pH = 7.4) to the electrochemical reduction of H_2O_2 at various concentrations. An obvious reduction peak could be seen from Fig. 7a with 1 mM H_2O_2 added to the electrochemical cell, and the peak current increased greatly compared to that without H_2O_2. The reduction peak current incresed with the increasing concentration of H_2O_2, indicating the

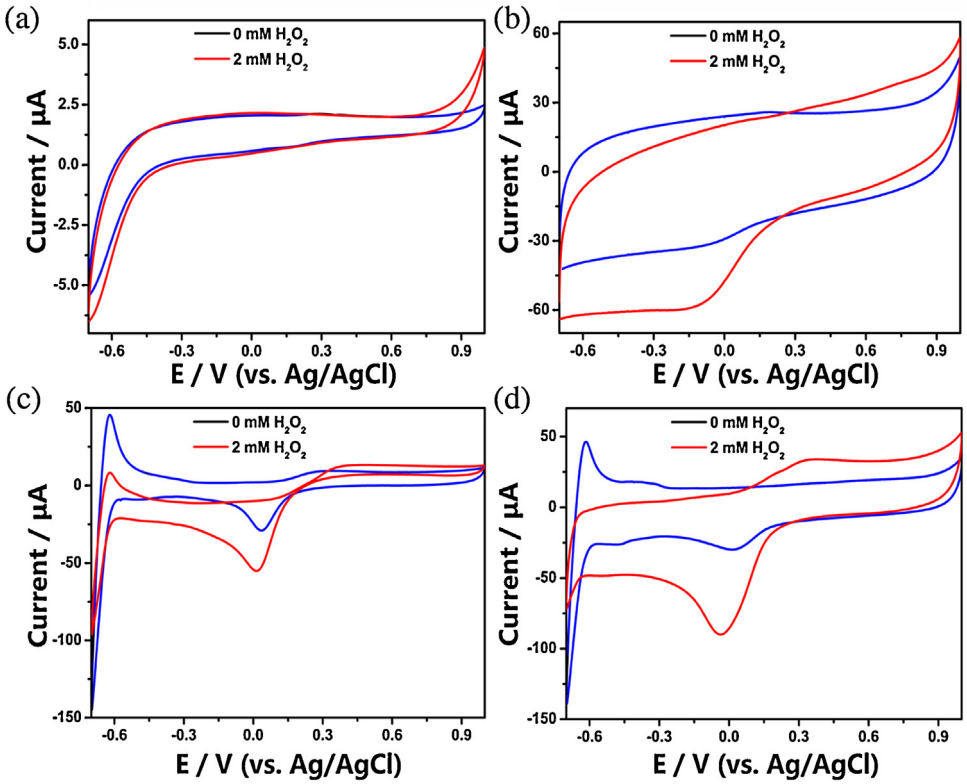

Fig. 6. Cyclic voltammograms (CVs) of (a) bare GCE, (b) pC_xN_{1-x}-modified GCE, (c) Pt-BNPs-modified GCE and (d) Pt-pC_xN_{1-x}-modified GCE in N_2-saturated 0.1 M PBS (pH = 7.4) in the absence and presence of 2 mM H_2O_2. Scan rate:50 mVs^{-1}.

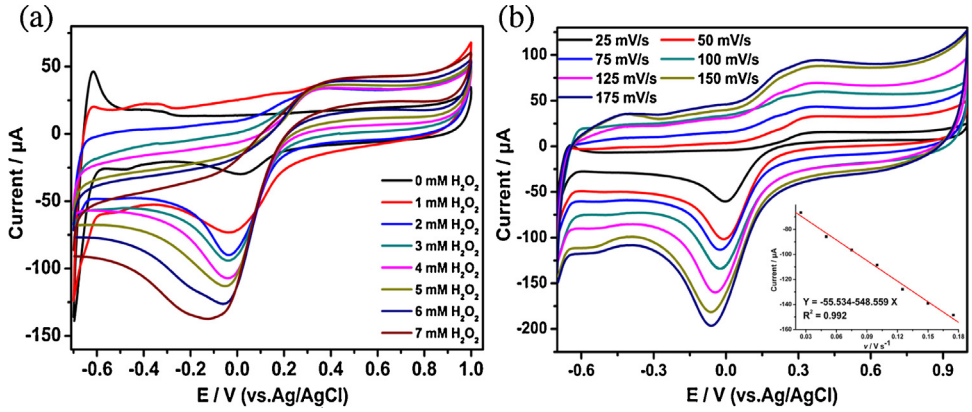

Fig. 7. (a) CVs of Pt-pC_xN_{1-x}-modified GCE in N_2-saturated 0.1 M PBS (pH = 7.4) containing different concentrations of H_2O_2 (0 mM, 1 mM, 2 mM, 3 mM, 4 mM, 5 mM, 6 mM, 7 mM). Scan rate: 50 mVs^{-1}. (b) CVs of 2 mM H_2O_2 on Pt-pC_xN_{1-x}-modified GCE in N_2-saturated 0.1 M PBS (pH = 7.4) at various scan rates: 25, 50,75, 100, 125, 150 and 175 mVs^{-1}. Inset is the calibration plot of the reduction peak current *vs.* the scan rate.

remarkable electrocatalytic activity of Pt-pC_xN_{1-x} on the electrode surface. Additionally, the peak potential remained basically unchanged with varying concentrations, showing the stability of Pt-pC_xN_{1-x}-modified GCE. Moreover, the electrocatalytic property of Pt-pC_xN_{1-x} to H_2O_2 reduction in CVs suggested that this excellent nanocomposite could be applied to the amperometric detection measurement.

The CVs of Pt-pC_xN_{1-x}-modified GCE in 0.1 M PBS (pH = 7.4) containing 2 mM H_2O_2 at various scan rates were also investigated. As shown in Fig. 7b, the reduction peak current increased linearly with increasing scan rate in the presence of H_2O_2. And the linear regression equation was expressed as: $I_{pc} = -55.534 - 548.559\, v/mV\, s^{-1}$ ($R^2 = 0.992$), suggesting that the electrocatalysis of H_2O_2 on Pt-pC_xN_{1-x}-modified electrode is a typical surface-controlled process. The results which could be used to predict the electrocatalysis of H_2O_2 on Pt-pC_xN_{1-x} in two steps: (1) H_2O_2 molecules were rapidly diffused and absorbed on the surface of nanocomposites; (2) the H_2O_2 was reduced on the surface of Pt-BNPs in the process of two-electron transfer, which can be facilitated by the noble metal electrocatalysts [48]. During the whole process, pC_xN_{1-x} not only acts as a support to prevent Pt-BNPs from aggregating, but also as the electron transfer channels to enhance electric conductivity between Pt-BNPs and electrode.

The good electrochemical properties of Pt-pC_xN_{1-x} nanocomposites could be attributed to the following three factors: the porous structure, the doping of nitrogen atoms and a larger number of ultrafine Pt-BNPs exposed to surface. Abundance of pores can enlarge the surface area for anchoring Pt-BNPs and preventing aggregation [20]. Meanwhile, the pores are interconnected into a network-like structure to provide good electrochemical contact area and ensure a rapid diffusion [27]. Furthermore, the doping of nitrogen atoms can improve electrocatalytic properties with efficient effect on the asymmetric spins and charged structures of carbon atoms [23]. Finally, as the catalytic activity of Pt-BNPs depends on the quantity and size [14,16], a large number of ultrafine Pt-BNPs can create more catalytic active sites for catalytic reduction of H_2O_2 and produce higher current response.

3.4. Amperometric response of the Pt-pC_xN_{1-x}-modified GCE to H_2O_2 reduction

As previously reported [23,45], the amperometric response of a modified electrode is closely linked with the applied potential, thus it is necessary to explore the effect of applied potentials. The amperometric signals of H_2O_2 on Pt-pC_xN_{1-x}-modified GCE at different applied working potentials under stirred conditions were shown in Fig. S6. The current responses at different potentials were close to each other, and the reduction current of H_2O_2 reached its highest at a potential of −0.02 V (Fig. S6). Hence, the optimized working potential was −0.02 V, which was adopted in the following amperometric *i-t* study.

The typical amperometric responses of different modified electrodes were investigated upon successive addition of varying concentrations of H_2O_2 in a continuous stirring PBS solution (0.1 M, pH = 7.4) at the optimized potential of −0.02 V. From Fig. 8a, it can

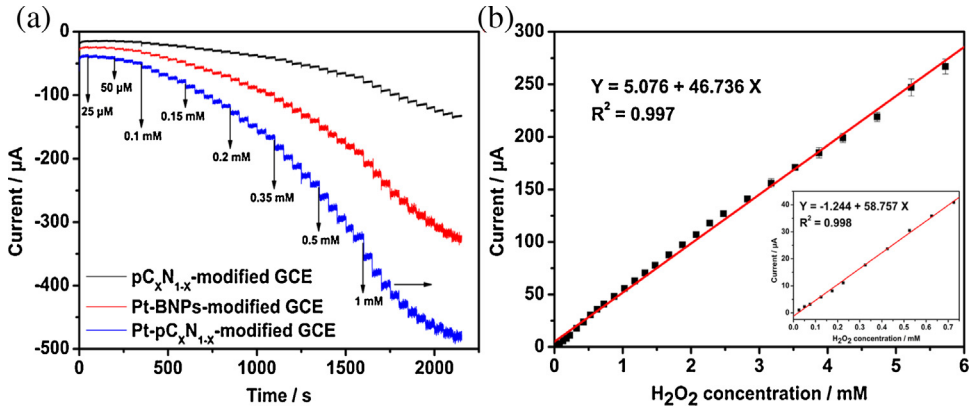

Fig. 8. (a) Current-time curve of pC_xN_{1-x}-modified GCE, Pt-BNPs-modified GCE and Pt-pC_xN_{1-x}-modified GCE upon successive addition of H_2O_2 to N_2-saturated 0.1 M PBS (pH = 7.4) at an applied potential of −0.02 V. (b)The calibration plot of electrocatalytic current versus different concentrations of H_2O_2 by Pt-pC_xN_{1-x}-modified GCE.

be clearly observed that all the three different modified electrodes responded rapidly and reached a steady signal within only 2 s upon the addition of H_2O_2. Compared with pC_xN_{1-x}-modified GCE and Pt-BNPs-modified GCE, Pt-pC_xN_{1-x}-modified GCE could achieve the maximum steadystate current under the same conditions, the electrocatalytic activity towards H_2O_2 reduction could be greatly enhanced by the compound of Pt-BNPs and pC_xN_{1-x}. Moreover, Pt-BNPs-modified GCE had a higher current response value than that of pC_xN_{1-x}-modified GCE due to the inherent high electrocatalytic activity of Pt-BNPs [2]. The Pt-pC_xN_{1-x}-modified GCE electrode displayed a good linear response to H_2O_2 (Fig. 8b). The corresponding linear range for detection H_2O_2 at Pt-pC_xN_{1-x}-modified GCE is from 0.025 mM to 5.725 mM, with a detection limit of 2.29 μM based on the equation of LOD = 3 σ/b, where b is the slope of the calibration curve and σ is the standard deviation of the blank solution [47,49]. The obtained electrochemical parameters of Pt-pC_xN_{1-x}-modified GCE including detection potential, linear range, and detection limit are compared with those of other reported H_2O_2 sensors (Table S2), revealing that Pt-pC_xN_{1-x}-modified GCE is extremely competitive and even outperforms several recent reported electrodes. Based on the aforementioned data, it can be concluded that the as-synthesized Pt-pC_xN_{1-x} with high density subnanometer-size Pt-BNPs has rapid current response, a wider linear range and relatively lower detection limit for the electrocatalytic reduction of H_2O_2. These results indicate that Pt-pC_xN_{1-x} is an excellent electroactive material for enhanced non-enzymatic electrochemical sensing.

The other physiological species, for example, citric acid (CA), ascorbic acid (AA), urea and glucose (GLU) and other carbohydrates, were also discussed to investigate the anti-interference ability of Pt-pC_xN_{1-x}. Additionally, they possibly reacting and generating interfering electrochemical signals during the process of H_2O_2 reduction [15]. As illustrated in Fig. 9, upon the addition of 1 mM H_2O_2, a remarkable current response appeared. With further addition of 0.1 mM CA and 0.1 mM GLU, the current responses of 0.1 mM H_2O_2 basically remained unchanged. After the second injection of 0.1 mM H_2O_2, the obvious amperometric response appeared again, and the same phenomenon was observed for the third and the fourth addition of 0.1 mM H_2O_2. However, no obvious amperometric response occurred with the addition of 0.1 mM sucrose, and a slight fluctuation of current response appeared with the injections of urea and AA. The results demonstrated the prominent anti-interference performance and high selectivity of Pt-pC_xN_{1-x} in practical detection of H_2O_2.

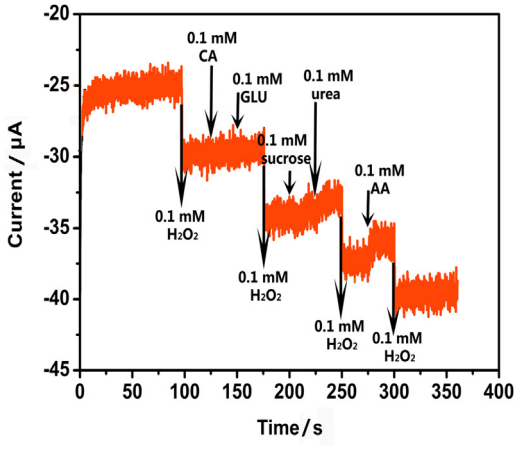

Fig. 9. Amperometric response of Pt-pC_xN_{1-x}-modified GCE in N_2-saturated 0.1 M PBS (pH = 7.4) to sequential addition of 0.1 mM H_2O_2, 0.1 mM CA, 0.1 mM GLU, 0.1 mM H_2O_2, 0.1 mM sucrose, 0.1 mM urea, 0.1 mM H_2O_2 and 0.1 mM AA at a working potential of −0.02 V.

Table 1
Amperometric determination of H_2O_2 in disinfected fetal bovine serum (FBS) samples (n = 10).

Sample	Added (μM)	Found (μM)	RSD (%)	Recovery (%)
1	25	25.11	1.4	100.43
2	50	49.82	1.2	99.65
3	100	101.37	2.3	101.37
4	200	204.13	1.9	102.07

The reproducibility of Pt-pC_xN_{1-x}-modified electrode was estimated by its responses to 2 mM H_2O_2 at several measurements for the same electrode and five different electrodes. The relative standard deviation (RSD) of the current signal for 2 mM H_2O_2 was 3.94% from five measurements for the same electrode. An acceptable RSD of 4.19% was acquired at five different modified electrodes prepared under the same conditions of current signals to 2 mM H_2O_2. The above results indicated that Pt-pC_xN_{1-x}-modified GCE has excellent reproducibility for the detection of H_2O_2. For the same Pt-pC_xN_{1-x}-modified GCE, the current response retained 93.6% of the initial value after a succession of 50 Cyclic Voltammetry cycles at 2 mM H_2O_2 (Fig. S7a). When the Pt-pC_xN_{1-x}-modified GCE was stored at 4 °C for one month, the current response to 2 mM H_2O_2 maintained about 83.0% of its original value (Fig. S7b), showing the good long-term stability of the Pt-pC_xN_{1-x}-modified GCE.

3.5. Real sample analysis

On the strength of good electrochemical performance, the feasibility of the proposed Pt-pC_xN_{1-x}-modified GCE for practical application was tested by detecting H_2O_2 in 1% disinfected fetal bovine serum (FBS) with the standard addition method. Based on the amperometric response of Pt-pC_xN_{1-x}-modified GCE, the concentration of H_2O_2 was obtained by the linear regression equation. And the recoveries of H_2O_2 with concentrations of 25 μM, 50 μM, 100 μM and 200 μM were obtained by the comparison of theoretical addition and determined concentration of H_2O_2. As shown in Table 1, the RSD of samples for ten successive measurements were all below 3.0%, which indicated the good reproducibility of Pt-pC_xN_{1-x}-modified GCE. These results showed that Pt-pC_xN_{1-x} possessed a good potential in determination of H_2O_2 in biological samples.

4. Conclusions

In this paper, the Pt-pC_xN_{1-x} was prepared by in situ synthesis through a one-step microwave-assisted heating procedure. The Pt-pC_xN_{1-x} reported here showed high activity for H_2O_2 detection. The functional Pt-pC_xN_{1-x} loaded subnanometer-size Pt-BNPs enrich edge and corner atoms which can efficiently catalyze the oxidation of the substrate TMB in the presence of H_2O_2. The lower K_m (K_m = 0.104) of Pt-pC_xN_{1-x} compared with HRP (K_m = 0.416) indicates its higher affinity with TMB in colorimetric reaction. The Pt-pC_xN_{1-x} also exhibited a better property for H_2O_2 electrochemical detection, with a low detection limit and wide linear region. Moreover, the reproducibility and stability of Pt-pC_xN_{1-x} were also superior and cost-effective for H_2O_2 electrochemical detection. Therefore, Pt-pC_xN_{1-x} can be developed as a unique and robust electrocatalyst for electrochemical biosensor applications.

Acknowledgements

We gratefully acknowledge the support for this research by National Natural Science Foundation of China (No. 21375043).

Appendix A. Supplementary data

Supplementary data associated with this article can be found, in the online version, at http://dx.doi.org/10.1016/j.electacta.2016.05.131.

References

[1] S. Guo, D. Wen, Y. Zhai, S. Dong, E. Wang, Platinum Nanoparticle Ensemble-on Graphene Hybrid Nanosheet: One-pot Rapid Synthesis, and Used as New Electrode Material for Electrochemical Sensing, ACS Nano 4 (2010) 3959.

[2] H. Wang, S. Li, Y. Si, N. Zhang, Z. Sun, H. Wu, Y. Lin, Platinum nanocatalysts loaded on graphene oxide-dispersed carbon nanotubes with greatly enhanced peroxidase-like catalysis and electrocatalysis activities, Nanoscale 6 (2014) 8107.

[3] L. Zhan, C. Li, W. Wu, C. Huang, A colorimetric immunoassay for respiratory syncytial virus detection based on gold nanoparticles–graphene oxide hybrids with mercury-enhanced peroxidase-like activity, Chem. Commun. 50 (2014) 11526.

[4] M.I. Kim, Y. Ye, M.A. Woo, J. Lee, H.G. Park, A highly efficient colorimetric immunoassay using a nanocomposite entrapping magnetic and platinum nanoparticles in ordered mesoporous carbon, Adv. Healthcare Mater. 3 (2014) 36.

[5] F. Pogacean, C. Socaci, S. Pruneanu, A.R. Biris, M. Coros, L. Magerusan, G. Katona, R. Turcu, G. Borodi, Graphene based nanomaterials as chemical sensors for hydrogen peroxide −A comparison study of their intrinsic peroxidase catalytic behavior, Sens. Actuators B-Chem. 213 (2015) 474.

[6] M.R. Mahmoudian, Y. Alias, W.J. Basirun, P.M. Woi, M. Sookhakian, Facile preparation of MnO_2 nanotubes/reduced graphene oxide nanocomposite for electrochemical sensing of hydrogen peroxide, Sens. Actuators B-Chem. 201 (2014) 526.

[7] L. Meng, Y. Xia, W. Liu, L. Zhang, P. Zou, Y. Zhang, Hydrogen microexplosion synthesis of platinum nanoparticles/nitrogen doped graphene nanoscrolls as new amperometric glucose biosensor, Electrochim. Acta 152 (2015) 330.

[8] O.G. Sahin, Microwave-assisted synthesis of PtAu@C based bimetallic nanocatalysts for non-enzymatic H_2O_2 sensor, Electrochim. Acta 180 (2015) 873.

[9] L.N. Zhang, H.H. Deng, F.L. Lin, X.W. Xu, S.H. Weng, A.L. Liu, X.H. Lin, X.H. Xia, W. Chen, In situ growth of porous platinum nanoparticles on graphene oxide for colorimetric detection of cancer cells, Anal. Chem. 86 (2014) 2711.

[10] W. He, Y. Liu, J. Yuan, J.J. Yin, X. Wu, X. Hu, K. Zhang, J. Liu, C. Chen, Y. Ji, Y. Guo, Au@Pt nanostructures as oxidase and peroxidase mimetics for use in immunoassays, Biomaterials 32 (2011) 1139.

[11] K. Cai, Z. Lv, K. Chen, L. Huang, J. Wang, F. Shao, Y. Wang, H. Han, Aqueous synthesis of porous platinum nanotubes at room temperature and their intrinsic peroxidase-like activity, Chem. Commun. 49 (2013) 6024.

[12] Y. Yu, Q. Sun, X. Liu, H. Wu, T. Zhou, G. Shi, Size-Controllable Gold-Platinum Alloy Nanoparticles on Nine Functionalized Ionic-Liquid Surfaces and Their Application as Electrocatalysts for Hydrogen Peroxide Reduction, Chem. Eur. J. 17 (2011) 11314.

[13] L. Wang, Y. Yamauchi, Block Copolymer Mediated Synthesis of Dendritic Platinum Nanoparticles, J. Am. Chem. Soc. 131 (2009) 9152.

[14] Y. Zuo, L. Wu, K. Cai, T. Li, W. Yin, D. Li, N. Li, J. Liu, H. Han, Platinum Dendritic-Flowers Prepared by Tellurium Nanowires Exhibit High Electrocatalytic Activity for Glycerol Oxidation, ACS Appl. Mater. Interfaces 7 (2015) 17725.

[15] H. Kivrak, O. Alal, D. Atbas, Efficient and rapid microwave-assisted route to synthesize Pt–MnO_x hydrogen peroxide sensor, Electrochim. Acta 176 (2015) 497.

[16] D. Zhao, B.Q. Xu, Enhancement of Pt utilization in electrocatalysts by using gold nanoparticles. Angew. Chem, Int. Ed. 45 (2006) 4955.

[17] Y. Yang, R. Fu, J. Yuan, S. Wu, J. Zhang, H. Wang, Highly sensitive hydrogen peroxide sensor based on a glassy carbon electrode modified with platinum nanoparticles on carbon nanofiber heterostructures, Microchim Acta 182 (2015) 2241.

[18] Z. Miao, D. Zhang, Q. Chen, Non-enzymatic Hydrogen Peroxide Sensors Based on Multi-wall Carbon Nanotube/Pt Nanoparticle Nanohybrids, Materials 7 (2014) 2945.

[19] L. Yan, X. Bo, D. Zhu, L. Guo, Well-dispersed Pt nanoparticles on polydopamine-coated ordered mesoporous carbons and their electrocatalytic application, Talanta 120 (2014) 304.

[20] J. Liu, X. Bo, Z. Zhao, L. Guo, Highly exposed Pt nanoparticles supported on porous graphene for electrochemical detection of hydrogen peroxide in living cells, Biosens. Bioelectron. 74 (2015) 71.

[21] P. Simon, Y. Gogotsi, Materials for electrochemical capacitors, Nat. Mater. 7 (2008) 845.

[22] X. Zheng, J. Luo, W. Lv, D.W. Wang, Q.H. Yang, Two-Dimensional Porous Carbon: Synthesis and Ion-Transport Properties, Adv. Mater. 27 (2015) 5388.

[23] Y. Meng, D. Voiry, A. Goswami, X. Zou, X. Huang, M. Chhowalla, Z. Liu, T. Asefa, N.- O.- and S-tridoped nanoporous carbons as selective catalysts for oxygen reduction and alcohol oxidation reactions, J. Am. Chem. Soc. 136 (2014) 13554.

[24] W.J. Lan, C.H. Chen, Hybridization of Graphene in 3D Complex Nanovoids: Synergistic Nanocomposites for Electrocatalytic Reduction of Hydrogen Peroxide, Electrochim. Acta 180 (2015) 1014.

[25] W. Shen, W. Fan, Nitrogen-containing porous carbons: synthesis and application, J. Mater. Chem. A. 1 (2013) 999.

[26] C.O. Ania, V. Khomenko, E. Raymundo-Piñero, J.B. Parra, F. Béguin, The Large Electrochemical Capacitance of Microporous Doped Carbon Obtained by Using a Zeolite Template, Adv. Funct. Mater. 17 (2007) 1828.

[27] Y. Qin, J. Yuan, J. Li, D. Chen, Y. Kong, F. Chu, Y. Tao, M. Liu, Crosslinking Graphene Oxide into Robust 3D Porous N-Doped Graphene, Adv. Mater. 27 (2015) 5171.

[28] Y. Wang, Y. Shao, D.W. Matson, J. Li, Y. Li, Nitrogen-Doped Graphene and Its Application in Electrochemical Biosensing, ACS Nano 4 (2010) 1790.

[29] M.T. Tajabadi, W.J. Basirun, F. Lorestani, R. Zakaria, S. Baradaran, Y.M. Amin, M. R. Mahmoudian, M. Rezayi, M. Sookhakian, Nitrogen-doped graphene-silver nanodendrites for the non-enzymatic detection of hydrogen peroxide, Electrochim. Acta 151 (2015) 126.

[30] Y. Zhou, K. Neyerlin, T.S. Olson, S. Pylypenko, J. Bult, H.N. Dinh, T. Gennett, Z. Shao, R. O'Hayre, Enhancement of Pt and Pt-alloy fuel cell catalyst activity and durability via nitrogen-modified carbon supports, Energy Environ. Sci. 3 (2010) 1437.

[31] Y. Zhou, R. Pasquarelli, T. Holme, J. Berry, D. Ginley, R. O'Hayre, Improving PEM fuel cell catalyst activity and durability using nitrogen-doped carbon supports: observations from model Pt/HOPG systems, J. Mater. Chem. 19 (2009) 7830.

[32] G. Yang, H. Han, T. Li, C. Du, Synthesis of nitrogen-doped porous graphitic carbons using nano-$CaCO_3$ as template, graphitization catalyst, and activating agent, Carbon 50 (2012) 3753.

[33] T. Li, G. Yang, J. Wang, Y. Zhou, H. Han, Excellent electrochemical performance of nitrogen-enriched hierarchical porous carbon electrodes prepared using nano-$CaCO_3$ as template, J. Solid State Electrochem. 17 (2013) 2651.

[34] T. Lin, L. Zhong, J. Wang, L. Guo, H. Wu, Q. Guo, F. Fu, G. Chen, Graphite-like carbon nitrides as peroxidase mimetics and their applications to glucose detection, Biosens. Bioelectron. 59 (2014) 89.

[35] X. Xu, S. Jiang, Z. Hu, S. Liu, Nitrogen-Doped Carbon Nanotubes: High Electrocatalytic Activity toward the Oxidation of Hydrogen Peroxide and Its Application for Biosensing, ACS Nano 4 (2010) 4292.

[36] S.K. Maji, S. Sreejith, A.K. Mandal, X. Ma, Y. Zhao, Immobilizing Gold Nanoparticles in Mesoporous Silica Covered Reduced Graphene Oxide: A Hybrid Material for Cancer Cell Detection through Hydrogen Peroxide Sensing, ACS Appl. Mater. Interfaces 6 (2014) 13648.

[37] Y. Song, K. Qu, C. Zhao, J. Ren, X. Qu, Graphene oxide: intrinsic peroxidase catalytic activity and its application to glucose detection, Adv. Mater. 22 (2010) 2206.

[38] F. Su, Z. Tian, C.K. Poh, Z. Wang, S.H. Lim, Z. Liu, J. Lin, Pt Nanoparticles Supported on Nitrogen-Doped Porous Carbon Nanospheres as an Electrocatalyst for Fuel Cells, Chem. Mater. 22 (2010) 832.

[39] L.M. Zhang, Z.B. Wang, J.J. Zhang, X.L. Sui, L. Zhao, D.M. Gu, Honeycomb-like mesoporous nitrogen-doped carbon supported Pt catalyst for methanol electrooxidation, Carbon 93 (2015) 1050.

[40] C. Xiao, Q. Zou, Y. Tang, Surface nitrogen-enriched carbon nanotubes for uniform dispersion of platinum nanoparticles and their electrochemical biosensing property, Electrochim. Acta 143 (2014) 10.

[41] X. Wen, D. Zhang, T. Yan, J. Zhang, L. Shi, Three-dimensional graphene-based hierarchically porous carbon composites prepared by a dual-template strategy for capacitive deionization, J. Mater. Chem. A. 1 (2013) 12334.

[42] A.C. Ferrari, J. Robertson, Interpretation of Raman spectra of disordered and amorphous carbon, Phys. Rev. B 61 (2000) 14095.

[43] W. Shi, Q. Wang, Y. Long, Z. Cheng, S. Chen, H. Zheng, Y. Huang, Carbon nanodots as peroxidase mimetics and their applications to glucose detection, Chem. Commun. 47 (2011) 6695.

[44] L. Gao, J. Zhuang, L. Nie, J. Zhang, Y. Zhang, N. Gu, T. Wang, J. Feng, D. Yang, Intrinsic peroxidase-like activity of ferromagnetic nanoparticles, Nat. Nanotechnol. 2 (2007) 577.

[45] Y. Zhang, X. Bai, X. Wang, K.-K. Shiu, Y. Zhu, H. Jiang, Highly Sensitive Graphene–Pt Nanocomposites Amperometric Biosensor and Its Application in Living Cell H_2O_2 Detection, Anal. Chem. 86 (2014) 9459.

[46] X. Li, X. Liu, W. Wang, L. Li, X. Lu, High loading Pt nanoparticles on functionalization of carbon nanotubes for fabricating nonenzyme hydrogen peroxide sensor, Biosens. Bioelectron. 59 (2014) 221.

[47] P. Moozarm Nia, F. Lorestani, W.P. Meng, Y. Alias, A novel non-enzymatic H_2O_2 sensor based on polypyrrole nanofibers–silver nanoparticles decorated reduced graphene oxide nano composites, Appl. Surf. Sci. 332 (2015) 648.

[48] D. Cao, L. Sun, G. Wang, Y. Lv, M. Zhang, Kinetics of hydrogen peroxide electroreduction on Pd nanoparticles in acidic medium, J. Electroanal. Chem. 621 (2008) 31.

[49] L. Wu, K. Chen, Z.T. Li, K. Shao, F. Shao, H. Han, Hydrogen-bonding recognition-induced aggregation of gold nanoparticles for the determination of the migration of melamine monomers using dynamic light scattering, Anal. Chim. Acta 845 (2014) 92.